Aggregating Flexibility of Heterogeneous Energy Resources in Distribution Networks

Tianyi Chen, Na Li, and Georgios B. Giannakis

***Abstract*—Distributed energy resources (DERs) in distribution networks have great potential for providing capacity reserves to the transmission systems. In this context, this paper focuses on optimizing the aggregated flexibility of DERs in power distribution networks, involving both network-wide voltage constraints, and individual device operating constraints. The intended task is first formulated as a convex program, and several critical properties of the underlying optimal aggregation solution are then highlighted via rigorous convex analysis. Leveraging the special problem structure, a decentralized solver is further developed to efficiently find the optimal aggregation trajectory with limited communication. Performance tests on the IEEE 37-bus benchmark are conducted to verify the theoretical findings and demonstrate the impact of various network configurations.**

I. Introduction

The bulk grid infrastructure is on the verge of a major paradigm shift to a cyber-enabled "smart" one. Among several attractive features, the smart grid will embrace renewable energy sources thanks to their environment-friendly and price-competitive advantages over conventional generation [2]. However, high penetration of renewables introduces new challenges for system operation, such as stringent requirement of ramping *flexibility* due to their high fluctuations [3].

To tackle this challenge, a prevalent solution is to harness the flexibility provided by distributed energy resources (DERs), such as photovoltaic (PV) systems, on-site energy storage and thermostatically controlled loads (TCLs). Most existing efforts in this discipline focus on real-time control of individual distribution-level DER devices to track a time-varying reference signal set by a transmission system operator such as Independent Service Operator (ISO) [4]–[7]. This is usually referred as *disaggregation*. In contrast, *aggregation* is a bottom-up procedure representing a collection of DERs as a single resource to the upper-level transmission system [8]. The idea is to allow the aggregator (e.g., feeder of a distribution network) to participate in the electricity markets, and provide auxiliary service as a *virtual power plant* by using the accumulated flexibility from individual devices. The challenges naturally arise due to the distribution network constraints, and the local device constraints such as the upper and lower limits of the energy-level in storage devices and temperature limits of TCLs [9]. Therefore, how to aggregate millions of kilowatt-level DERs in distribution networks into the gigawatt-level power dispatch in transmission networks remains to be explored [3].

Related work. Our motivation here is to thoroughly understand how much flexibility the distribution-level DERs can provide within a dispatch horizon. A few recent efforts have been put forth to study the optimal flexibility aggregation task [3], [8]–[11]. Specifically, security-aware flexibility management between *transmission-level* systems was studied in [9], and an efficient coordination protocol was proposed therein. Targeting a succinct representation of aggregate TCLs profiles in distribution systems, a simple yet effective "virtual" battery model was developed in [10]. Leveraging such models, a geometric approach was put forth in [11] to obtain the feasible trajectories of virtual batteries with affordable complexity. Yet, the approaches in [10], [11] mainly focus on *modeling* specific DERs (e.g., TCLs), and the effect of network constraints in the distribution systems has not been considered. Real-time aggregation of flexible resources was studied in [8], with the goal of developing a light-weight scheme suitable for running on millisecond time scale. In a recent work [3], flexibility aggregation was studied in the context of multi-period OPF, where heterogeneous constraints for local devices and distribution networks were considered. However, the structure of the optimal solution and the performance limit have not been explored, and the decentralized solver has not been developed.

Our contributions. The *primary goal* of this paper is to conduct a comprehensive study on the aggregate flexibility provided by DERs, along with development of decentralized solvers for finding the feasible trajectories of interest.

Relative to existing work, the main contributions of the paper are summarized as follows.

c1) We formulate the optimal flexibility aggregation problem in the distribution network as a convex program, and further establish several elegant properties of it characterizing the optimal aggregation solution (Section III).

c2) Leveraging the problem structure, we develop an efficient decentralized solver based on the *predictor-corrector proximal multiplier* algorithm, which finds the optimal aggregation solution using local computation and communication (Section IV).

c3) Simulations based on the IEEE 37-bus benchmark and real load and PV data verify our theoretical findings, and demonstrate the impact of different network configurations on the performance (Section V).

II. Grid Modeling Preliminaries

Consider a distribution network represented by a graph $\mathcal{G} = (\mathcal{N}_0, \mathcal{E})$, where the set of nodes $\mathcal{N}_0$ corresponds to $N+1$ buses, and the edges in $\mathcal{E}$ correspond to E distribution lines [12]. The feeder bus is indexed by 0, whereas every non-feeder bus is $n \in \mathcal{N} := \{1, \ldots, N\}$. Thus, we have $\mathcal{N}_0 := \mathcal{N} \bigcup \{0\}$. The time is discrete and indexed by t within a finite time horizon $\mathcal{T} := \{1, \ldots, T\}$. The duration of a time slot could either coincide with realtime market periods (e.g., 5 minutes), or be even shorter (30 seconds), depending on the variability of

T. Chen and G. B. Giannakis are with the Dept. of Elec. & Comput. Engr. and the Digital Technology Center, University of Minnesota. Emails: chen3827, georgiosg@umn.edu. N. Li is affiliated with John A. Paulson School of Engineering and Applied Sciences at Harvard University. Email: nali@seas.harvard.edu. Work in this paper was supported by NSF 1442686, 1509040, 1548204, 1608509, and NSF CAREER 1553407. The work was also supported by Advanced Research Projects Agency-Energy (ARPA-E NODES). The proofs can be found in our online version [1].

active powers and cyber resources (sensing, communication, and computation delays) [2], [4].

Power flow models. Per bus $n \in \mathcal{N}$, let v_n be the squared voltage magnitude, and $p_n + jq_n$ the complex power injected to the network through the bus. For brevity, we use vectors $\mathbf{s}_n := [p_n, q_n]^\top$, and $\mathbf{s} := [\mathbf{s}_1^\top, \ldots, \mathbf{s}_N^\top]^\top$. Time subscript t will be included whenever needed; e.g., $\mathbf{s}_{n,t}$ and $\mathbf{s}_t$. We assume that power distribution networks have a tree structure with the feeder as their root. Let $\pi(n)$ denote the unique parent bus of bus n. We will simply index the edge $(\pi(n), n)$ as n, and the power flow on edge n seen at the sending bus $\pi(n)$ will be denoted by $P_{n,t} + jQ_{n,t}$ with $\mathbf{S}_n := [P_n, Q_n]^\top$. We adopt the linear approximation of the branch flow model[1] [5]

$$p_{n,t} = \sum_{k \in \mathcal{C}_n} P_{k,t} - P_{n,t} \tag{1a}$$

$$q_{n,t} = \sum_{k \in \mathcal{C}_n} Q_{k,t} - Q_{n,t} \tag{1b}$$

$$v_{n,t} = v_{\pi(n),t} - 2(r_n P_{n,t} + x_n Q_{n,t}) \tag{1c}$$

$$\underline{v}_n \leq v_{n,t} \leq \bar{v}_n \tag{1d}$$

where $\mathcal{C}_n$ denotes the set of the children nodes for bus n, $r_n + jx_n$ the impedance on line n, and $\underline{v}_n, \bar{v}_n$ denote the limits of voltage square magnitudes. For the feeder (root) bus 0, we use $p_{0,t}$ and $q_{0,t}$ to denote the active and reactive injections to the external grid. The following supply-demand equations hold:

$$p_{0,t} = \sum_{n \in \mathcal{N}} p_{n,t} \quad \text{and} \quad q_{0,t} = \sum_{n \in \mathcal{N}} q_{n,t}. \tag{2}$$

If $p_{0,t} > 0$ ($q_{0,t} > 0$), the distribution network generates active (reactive) power, otherwise, it consumes power. The active and reactive power injection at bus n can be decomposed into its generation and consumption components as

$$p_{n,t} = p^g_{n,t} - p^c_{n,t}; \quad q_{n,t} = q^g_{n,t} - q^c_{n,t}, \quad \forall n \in \mathcal{N}. \tag{3}$$

The following sections will specify these components, along with their operational constraints.

Power consumption includes non-controllable (e.g., illumination demand from residential areas), and controllable loads (e.g., demand from data centers and electric vehicles).

Non-controllable loads. For bus n with non-controllable loads, the consumed active power is given by $p^c_{n,t} \geq 0$, and its reactive power $q^c_{n,t} \geq 0$ is typically proportional to $p^c_{n,t}$ via a constant factor. Both $p^c_{n,t}$ and $q^c_{n,t}$ can not be changed.

Controllable loads. In contrast to non-controllable loads that must be satisfied per slot, the controllable loads at buses $\mathcal{N}_{\rm cl}$ provide some flexibility in power dispatch. For bus $n \in \mathcal{N}_{\rm cl}$ with controllable loads, denote the consumed active power as $p^c_{n,t}$, and its reactive power $q^c_{n,t}$, both of which can be adjusted but confined in a bounded interval, given by

$$\underline{p}^c_{n,t} \leq p^c_{n,t} \leq \bar{p}^c_{n,t}, \quad \underline{q}^c_{n,t} \leq q^c_{n,t} \leq \bar{q}^c_{n,t} \tag{4}$$

where $\bar{p}^c_{n,t}$ ($\bar{q}^c_{n,t}$) and $\underline{p}^c_{n,t}$ ($\underline{q}^c_{n,t}$) are pre-defined upper and lower limits for active (reactive) loads.

PV systems. If bus $n \in \mathcal{N}_{\rm pv}$ corresponds to a PV system, it generates active power with capacity over the interval $[\underline{p}^g_{n,t}, \bar{p}^g_{n,t}]$ and its inverter has capability $\bar{s}_n$. Here, $\underline{p}^g_{n,t}$ and $\bar{s}_n$ are pre-determined constants, that e.g., depend on device constraints, while $\bar{p}^g_{n,t}$ is given by the on-site PV availability. Thus, the *controllable* PV power generation $p^g_{n,t}$ and $q^g_{n,t}$ obey

$$\underline{p}^g_{n,t} \leq p^g_{n,t} \leq \bar{p}^g_{n,t}, \ (p^g_{n,t})^2 + (q^g_{n,t})^2 \leq (\bar{s}_n)^2, \ \forall n \in \mathcal{N}_{\rm pv}. \tag{5}$$

If the voltage constraint (1c) is not considered, the PV device simply obeys $\underline{p}^g_{n,t} \leq p^g_{n,t} \leq w_{n,t}$, with $w_{n,t} := \min\{\bar{p}^g_{n,t}, \bar{s}_n\}$.

Energy storage devices. If bus $n \in \mathcal{N}_{\rm bt}$ corresponds to an energy storage device e.g., a battery, it can act either as power generator ($p^g_{n,t} \geq 0$) or as consumer ($p^g_{n,t} < 0$) [13]. If $b_{n,t}$ represents the battery's state of charge (SOC) at the beginning of period t, the controllable generation $p^g_{n,t}$ and $q^g_{n,t}$ satisfy

$$b_{n,t+1} = b_{n,t} - \delta_T p^g_{n,t}, \quad \underline{b}_n \leq b_{n,t} \leq \bar{b}_n \tag{6a}$$

$$(p^g_{n,t})^2 + (q^g_{n,t})^2 \leq (\bar{s}_n)^2, \ \ \forall n \in \mathcal{N}_{\rm bt}, t \in \mathcal{T} \tag{6b}$$

where δ_T is the slot duration, and $\bar{s}_n$ is the capacity of battery at bus n. Constraints (6) capture the battery dynamics over consecutive slots as well as the SOC within the allowable levels $[\underline{b}_n, \overline{b_n}]$. To simplify analysis, we assume the (dis)charging coefficients to be 1 in (6a), which also appears in [13], [14].

For the notational brevity, we will further assume that each bus is associated with a single controllable power device either power load or generation. But the ensuing formulation, analysis and decentralized algorithm can be readily generalized to the case with multiple devices at each bus.

Aggregate flexibility. To quantify the system flexibility, we define two trajectories of power injections at each bus of the distribution network over the given horizon $\mathcal{T}$, given by the active injections $\mathbf{p}^{\rm up}_t := [p^{\rm up}_{1,t}, \ldots, p^{\rm up}_{N,t}]^\top$ and $\mathbf{p}^{\rm low}_t := [p^{\rm low}_{1,t}, \ldots, p^{\rm low}_{N,t}]^\top$, along with the reactive ones $\mathbf{q}^{\rm up}_t$ and $\mathbf{q}^{\rm low}_t$. Accordingly, the complex power trajectories are $\mathbf{s}^{\rm up}_t := [(\mathbf{p}^{\rm up}_t)^\top, (\mathbf{q}^{\rm up}_t)^\top]^\top$, and $\mathbf{s}^{\rm low}_t := [(\mathbf{p}^{\rm low}_t)^\top, (\mathbf{q}^{\rm low}_t)^\top]^\top$. The corresponding active power injections from the distribution network to grid are $p^{\rm up}_{0,t}$ and $p^{\rm low}_{0,t}$, and obey the following conservation law (cf. (2))

$$p^{\rm up}_{0,t} = \sum_{n \in \mathcal{N}} p^{\rm up}_{n,t} \quad \text{and} \quad p^{\rm low}_{0,t} = \sum_{n \in \mathcal{N}} p^{\rm low}_{n,t}. \tag{7}$$

The generic variables $\{p_{n,t}\}$ are used in (1)-(6), but whenever appropriate, they should be understood as $\{p^{\rm up}_{n,t}\}$ for the upper trajectory, and likewise $\{p^{\rm low}_{n,t}\}$ for the lower trajectory.

The *system flexibility* is determined by the difference between the aggregated power injections (negative power consumptions) of the distribution network under the *upper* and *lower* trajectories; that is, the difference between $p^{\rm up}_{0,t}$ and $p^{\rm low}_{0,t}$; see e.g., Fig. 1. Utility of such a figure of merit will be evaluated by a (possibly time-varying) concave function of the power injection difference $p^{\rm up}_{0,t} - p^{\rm low}_{0,t}$, given by $\sum_{t=1}^T f(p^{\rm up}_{0,t} - p^{\rm low}_{0,t})$. Intuitively, this function should be a nondecreasing function of flexibility $p^{\rm up}_{0,t} - p^{\rm low}_{0,t}$. An interesting choice of the objective corresponds to the logarithmic function of $p^{\rm up}_{0,t} - p^{\rm low}_{0,t}$, namely

$$\sum_{t=1}^T f(p^{\rm up}_{0,t} - p^{\rm low}_{0,t}) := \sum_{t=1}^T \log\left(p^{\rm up}_{0,t} - p^{\rm low}_{0,t}\right). \tag{8}$$

Clearly, maximizing (8) is tantamount to maximizing the *volume* of the tube between two trajectories $\{p^{\rm up}_{0,t}\}$ and $\{p^{\rm low}_{0,t}\}$;

[1]The power flow model can be replaced by more complicated models, such as the nonlinear branch flow model, or other linear models in [6].

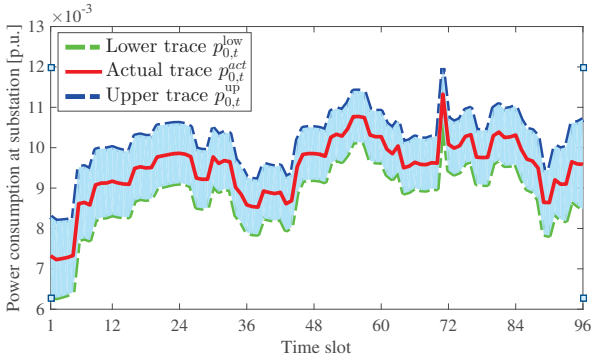

Fig. 1. An example of optimal upper and lower trajectories. The shaded region represents the range of all feasible trajectories, including $\{p^{\text{act}}_{0,t}\}$ from the actual transmission-level power dispatch.

that is, $\prod_{t=1}^{T}\left(p^{\text{up}}_{0,t}-p^{\text{low}}_{0,t}\right)$. In addition, the log function can ensure fairness across slots because for a fixed total amount of $\sum_t^T y_t$, maximizing $\sum_t^T \log(y_t)$ will lead to equally allocating y_t per slot. If the system aggregator would choose to prioritize flexibility on certain time slots, the aggregator can introduce weight factors $\{u_t\}$ and modify the objective to maximize $\sum_t^T u_t \log(p^{\text{up}}_{0,t}-p^{\text{low}}_{0,t})$.

III. Flexibility Aggregation via Convex Optimization

Building on the system model of Section II, we formulate the problem and analyze the optimal solution in this section.

A. Problem statement

With the local constraints and objective in mind, the overall goal of the network operator is to find the upper and lower trajectories $\{\mathbf{s}^{\text{up}}_t,\mathbf{s}^{\text{low}}_t\}_{t=1}^T$ to maximize the system flexibility in terms of the aggregated active power at the substation, subject to local constraints. Concretely, we aim at solving the following *aggregation* problem

$$f^*:=\max_{\{\mathbf{s}^{\text{up}}_t,\mathbf{s}^{\text{low}}_t\}}\ \sum_{t=1}^{T} f\left(p^{\text{up}}_{0,t}-p^{\text{low}}_{0,t}\right) \tag{9a}$$

$$\text{s.to}\quad \mathbf{s}^{\text{up}}_t\geq\mathbf{s}^{\text{low}}_t,\quad \forall t\in\mathcal{T} \tag{9b}$$

$$(1)-(6) \tag{9c}$$

where the generic variables in (1)-(6) should be augmented with subscript *up* or *low* indicating trajectories $\{\mathbf{s}^{\text{up}}_t\}$ or $\{\mathbf{s}^{\text{low}}_t\}$. The objective (9a) is concave, and the constraints (9b)-(9c) define a convex feasible set; hence, (9) is a convex program. Available convex programming solvers such as the gradient-type (or interior-point) iterative algorithms can be employed to solve the problem in a centralized fashion. And the optimal solution of (9) essentially contains the upper and lower aggregate traces shown in Fig. 1.

Notice that we introduce a monotonic constraint (9b) in (9) to guarantee that any aggregate trajectory within the shaded region of Fig. 1 is achievable by properly coordinating local devices in real-time power balancing. The next theorem will formally establish the existence of feasible *disaggregation* solutions given aggregate power trajectories.

Theorem 1. *Consider the problem* (9) *and the corresponding optimal trajectories* $\{\mathring{\mathbf{s}}^{\text{up}}_t,\mathring{\mathbf{s}}^{\text{low}}_t\}_{t=1}^T$. *For any aggregation trajectory* $\{\tilde{p}_{0,t}\}_{t=1}^T$ *at the substation satisfying*

$$\mathring{p}^{\text{up}}_{0,t}\geq\tilde{p}_{0,t}\geq\mathring{p}^{\text{low}}_{0,t},\ \forall t\in\mathcal{T} \tag{10}$$

there exists a disaggregation trajectory $\{\tilde{\mathbf{s}}_t\}_{t=1}^T$ *that is feasible with respect to* (1)-(6)*, namely, there exist* $\{p_{n,t},q_{n,t},P_{n,t},Q_{n,t},v_{n,t}\}$ *satisfying*

$$\tilde{p}_{0,t}=\sum_{n\in\mathcal{N}}p_{n,t} \tag{11a}$$

$$(1),(3)-(6). \tag{11b}$$

Building on the aggregation problem defined in this section, we will proceed to explore the underlying structure of the optimal solution along with its performance limit.

B. Optimal aggregation policy

To begin with, we use the following definitions to describe the planned trajectories $\{\mathbf{s}^{\text{up}}_t,\mathbf{s}^{\text{low}}_t\}_{t=1}^T$. Specifically, the planned trajectories are [15]

- d1) *feasible*, if $\{\mathbf{s}^{\text{up}}_t,\mathbf{s}^{\text{low}}_t\}_{t=1}^T$ satisfy (9b)-(9c);
- d2) *optimal*, if $\{\mathbf{s}^{\text{up}}_t,\mathbf{s}^{\text{low}}_t\}_{t=1}^T$ are feasible, and yield the optimal objective f^* in (9a); and
- d3) *water-filling*, if $\{\mathbf{s}^{\text{up}}_t,\mathbf{s}^{\text{low}}_t\}_{t=1}^T$ are feasible, and satisfy

$$p^{\text{low}}_{0,t}-p^{\text{up}}_{0,t}=[W-R_t]^+ + R_t\ ,\forall t\in\mathcal{T} \tag{12}$$

where $W\in\mathbb{R}$ is some constant, and $R_t:=\sum_{n\in\mathcal{N}_{\text{pv}}\cup\mathcal{N}_{\text{cl}}}(p^{\text{up}}_{n,t}-p^{\text{low}}_{n,t})$.

Before formally establishing the structure of optimal policies, we assume that the following condition are satisfied.

Assumption 1. *For every* t*, the objective function* $f(\cdot)$ *is strongly concave, and increasing.*

Assumption 2. *There exist trajectories* $\{\mathbf{s}^{\text{up}}_t,\mathbf{s}^{\text{low}}_t\}$ *that are feasible w.r.t.* (9)*, and satisfy* $b^{\text{up}}_{n,T+1}=\underline{b}_n$*, and* $b^{\text{low}}_{n,T+1}=\bar{b}_n$.

Note that Assumption 1 is readily satisfied by e.g., a quadratic or a logarithmic objective in (8); and, Assumption 2 holds also without sacrificing much generality. Relying on these desirable properties, the next lemma argues that the water-filling solution would be an appealing solution.

Lemma 1. *For* (9)*, if* $\{\mathbf{s}^{\text{up}}_t,\mathbf{s}^{\text{low}}_t\}$ *admit the water-filling structure (cf.* (12)*) and satisfy* $\sum_{t\in\mathcal{T}}(p^{\text{up}}_{n,t}-p^{\text{low}}_{n,t})=\bar{b}_n-\underline{b}_n$*, the battery operations are optimal given the current trajectories of other controllable devices* $\{p^{\text{up}}_{n,t},p^{\text{low}}_{n,t},n\in\mathcal{N}_{\text{pv}}\cup\mathcal{N}_{\text{cl}}\}$.

Although Lemma 1 does not admit a closed-form solution due to intertwined physical constraints, it unveils a concise yet fundamental insight. Specifically, complementing the flexibility provided by PV and controllable loads, the energy storage devices can adapt their (dis)charging operations to fill the *flexibility valley* (low flexibility), thus smoothing the temporal curve of aggregate flexibility. In other words, while the flexibility provided by PV and flexible loads is instantaneous and variable, the batteries mitigate the temporal variability to offer stationary capacity reserves. This water-filling structure is numerically shown in Figs. 2(c), 3(c), 6 and 8 of Section V.

With the insights gained on the optimal aggregation at substation level, the next lemma characterizes the optimal

behavior of individual devices. Let us term (9) without voltage constraints (1d) as the *simplified* problem

$$\tilde{f}^* := \max_{\{\mathbf{s}_t^{\rm up}, \mathbf{s}_t^{\rm low}\}} \sum_{t=1}^{T} f\left(p_{0,t}^{\rm up} - p_{0,t}^{\rm low}\right) \quad (13a)$$

$$\text{s.to} \quad (1a)-(1b),\ (3)-(6),\ (9b). \quad (13b)$$

Different from (9), the feasible set of (13) does not include *coupled* constraints across the network. Therefore, it reveals a neat optimal solution for each device highlighted next.

Lemma 2. *Considering the problem* (13) *and the optimal trajectories* $\{\mathring{\mathbf{s}}_t^{\rm up}, \mathring{\mathbf{s}}_t^{\rm low}\}$*, the following statement holds:*

- *s1) the optimal PV injections are* $\mathring{p}_{n,t}^{\rm g,low} = \underline{p}_{n,t}^{g}$*, and* $\mathring{p}_{n,t}^{\rm g,up} = \min\{\bar{p}_{n,t}^{g}, \bar{s}_n\}$*,* $\forall n \in \mathcal{N}_{\rm pv}$*;*
- *s2) the optimal controllable loads are* $\mathring{p}_{n,t}^{\rm c,low} = \bar{p}_{n,t}^{c}$*, and* $\mathring{p}_{n,t}^{\rm c,up} = \underline{p}_{n,t}^{c}$*,* $\forall n \in \mathcal{N}_{\rm cl}$*; and,*
- *s3) at the end of the time horizon, the energy levels of batteries under the optimal trajectories are given by* $\mathring{b}_{n,T+1}^{\rm up} = \underline{b}_n$*, and* $\mathring{b}_{n,T+1}^{\rm low} = \bar{b}_n$*,* $\forall n \in \mathcal{N}_{\rm pv}$*.*

Lemma 2 characterizes the optimal local operations by unfolding the optimal global trajectories, most of which also meet our intuition. Although Lemma 2 is for (13) that does not include the voltage constraints, it still provides useful information about the behavior of individual devices, especially when the voltage constraints are not binding.

Combining Lemmas 1 and 2, we can readily reach the following conclusion.

Theorem 2. *Under the conditions of Lemma 1, if the constant in the water-filling solution* $\{\mathbf{s}_t^{\rm up}, \mathbf{s}_t^{\rm low}\}$ *is given by (cf.* (12)*)*

$$R_t := \sum_{n\in\mathcal{N}_{\rm pv}} (\min\{\bar{p}_{n,t}^{g}, \bar{s}_n\} - \underline{p}_{n,t}^{g}) + \sum_{n\in\mathcal{N}_{\rm cl}} (\bar{p}_{n,t}^{c} - \underline{p}_{n,t}^{c}) \quad (14)$$

they are the optimal trajectories of (9)*.*

Before delving to algorithmic issues, we next establish the maximum flexibility of the distribution network.

Proposition 1. *The fundamental limit of the average system flexibility (in the sense of* (9a)*) is given by*

$$\frac{1}{T}\sum_{t=1}^{T} f\left(p_{0,t}^{\rm up} - p_{0,t}^{\rm low}\right) \le f\left(\frac{1}{T}\sum_{n\in\mathcal{N}_{\rm bt}} (\bar{b}_n - \underline{b}_n)/\delta_T + \frac{1}{T}\sum_{t\in\mathcal{T}} (\Delta p_t^{\rm pv} + \Delta p_t^{\rm cl})\right) \quad (15)$$

which depends on the maximum flexibility from PV generation $\Delta p_t^{\rm pv} := \sum_{n\in\mathcal{N}_{\rm pv}} (\bar{p}_{n,t}^{g} - \underline{p}_{n,t}^{g})$*, from controllable loads* $\Delta p_t^{\rm cl} := \sum_{n\in\mathcal{N}_{\rm cl}} (\bar{p}_{n,t}^{c} - \underline{p}_{n,t}^{c})$*, and the aggregate battery capacity.*

Proposition 1 asserts that the aggregate flexibility of a power distribution network is uniformly upper bounded under all possible trajectories of (re-)active power injections at all buses. When the local operating conditions of heterogeneous devices (e.g., batteries, PV inverters, and appliances) vary, the limit of the aggregate flexibility only depends on the flexible portion of PV generation and loads, as well as the aggregate battery capacity. From a system design perspective, this bound provides practical guidance to increase the operational flexibility.

IV. Decentralized flexibility aggregation solvers

A decentralized solver will be developed here for the optimal flexibility aggregation in (9). With voltage constraint (1c), (9) is challenging since the objective and the constraints couple the power injections at all the buses. Observe that the constraints that couple decision variables across buses are (1) and (2), while the active power constraint in (2) can be merged into (1a) by letting $p_{0,t} + \sum_{k\in\mathcal{C}_0} P_{k,t} = 0$. Leveraging this structure, we will develop a decentralized solver using the *predictor-corrector proximal multiplier* (PCPM) method[2] [17].

Consider the dual variables $\{\boldsymbol{\alpha}_t\}$, $\{\boldsymbol{\gamma}_t\}$, and $\{\boldsymbol{\nu}_t\}$ associated with the **a**ctive, **r**eactive, and **v**oltage constraints (1a)-(1c), respectively. With superscripts denoting the upper and lower trajectories, they are $\{\boldsymbol{\alpha}_t^{\rm up}, \boldsymbol{\gamma}_t^{\rm up}, \boldsymbol{\nu}_t^{\rm up}, \boldsymbol{\alpha}_t^{\rm low}, \boldsymbol{\gamma}_t^{\rm low}, \boldsymbol{\nu}_t^{\rm low}\}$. With proper initialization, the PCPM algorithm operates in the following three steps: dual prediction, primal correction, and dual correction. Specifically, at each iteration τ, the **dual prediction** is given by (stepsize $\mu > 0$)

$$\begin{aligned}
\hat{\alpha}_{0,t} &= \alpha_{0,t}(\tau) + \mu\left(p_{0,t}(\tau) + \textstyle\sum_{k\in\mathcal{C}_0} P_{k,t}(\tau)\right) \quad (16)\\
\hat{\alpha}_{n,t} &= \alpha_{n,t}(\tau) + \mu\left(p_{n,t}(\tau) - \textstyle\sum_{k\in\mathcal{C}_n} P_{k,t}(\tau) + P_{n,t}(\tau)\right)\\
\hat{\gamma}_{n,t} &= \gamma_{n,t}(\tau) + \mu\left(q_{n,t}(\tau) - \textstyle\sum_{k\in\mathcal{C}_n} Q_{k,t}(\tau) + Q_{n,t}(\tau)\right)\\
\hat{\nu}_{n,t} &= \nu_{n,t}(\tau) + \mu\big(v_{n,t}(\tau) - v_{\pi(n),t}(\tau) + 2r_n P_{n,t}(\tau) + 2x_n Q_{n,t}(\tau)\big)
\end{aligned}$$

where $\{\hat{\alpha}_{n,t}, \hat{\gamma}_{n,t}, \hat{\nu}_{n,t}\}$ are auxiliary variables, and (16) is repeated for multipliers with both *upper* and *lower* trajectories.

The **primal correction** at the substation is (stepsize $\eta > 0$)

$$\min_{\{p_{0,t}^{\rm low}, p_{0,t}^{\rm up}\}} \sum_{t=1}^{T} \Big(f\left(p_{0,t}^{\rm up} - p_{0,t}^{\rm low}\right) + \hat{\alpha}_{0,t}^{\rm up} p_{0,t}^{\rm up} + \hat{\alpha}_{0,t}^{\rm low} p_{0,t}^{\rm low} + \frac{1}{2\eta}\left(p_{0,t}^{\rm up} - p_{0,t}^{\rm up}(\tau)\right)^2 + \frac{1}{2\eta}\left(p_{0,t}^{\rm low} - p_{0,t}^{\rm low}(\tau)\right)^2 \Big) \quad (17)$$

and the correction step at each bus n is given by

$$\begin{aligned}
\min_{\text{(1d),(3)}-\text{(6),(9b)}} \sum_{t=1}^{T} \Big(& \hat{\alpha}_{n,t}^{\rm up}(p_{n,t}^{\rm up} + P_{n,t}^{\rm up}) + \hat{\alpha}_{n,t}^{\rm low}(p_{n,t}^{\rm low} + P_{n,t}^{\rm low})\\
& - \hat{\alpha}_{\pi(n),t}^{\rm up} P_{n,t}^{\rm up} - \hat{\alpha}_{\pi(n),t}^{\rm low} P_{n,t}^{\rm low} + \hat{\gamma}_{n,t}^{\rm up}(q_{n,t}^{\rm up} + Q_{n,t}^{\rm up}) + \hat{\gamma}_{n,t}^{\rm low}(q_{n,t}^{\rm low} + Q_{n,t}^{\rm low})\\
& - \hat{\gamma}_{\pi(n),t}^{\rm up} Q_{n,t}^{\rm up} - \hat{\gamma}_{\pi(n),t}^{\rm low} Q_{n,t}^{\rm low} + \hat{\nu}_{n,t}^{\rm up}(v_{n,t}^{\rm up} + 2r_n P_{n,t}^{\rm up} + 2x_n Q_{n,t}^{\rm up})\\
& + \hat{\nu}_{n,t}^{\rm low}(v_{n,t}^{\rm low} + 2r_n P_{n,t}^{\rm low} + 2x_n Q_{n,t}^{\rm low}) - \textstyle\sum_{k\in\mathcal{C}_n} \hat{\nu}_{k,t}^{\rm low} v_{n,t}^{\rm low}\\
& - \textstyle\sum_{k\in\mathcal{C}_n} \hat{\nu}_{k,t}^{\rm up} v_{n,t}^{\rm up} + \frac{1}{2\eta}\left(v_{n,t}^{\rm up} - v_{n,t}^{\rm up}(\tau)\right)^2 + \frac{1}{2\eta}\left(v_{n,t}^{\rm low} - v_{n,t}^{\rm low}(\tau)\right)^2\\
& + \tfrac{1}{2\eta}\left\|\mathbf{s}_{n,t}^{\rm up} - \mathbf{s}_{n,t}^{\rm up}(\tau)\right\|^2 + \tfrac{1}{2\eta}\left\|\mathbf{s}_{n,t}^{\rm low} - \mathbf{s}_{n,t}^{\rm low}(\tau)\right\|^2\\
& + \tfrac{1}{2\eta}\left\|\mathbf{S}_{n,t}^{\rm up} - \mathbf{S}_{n,t}^{\rm up}(\tau)\right\|^2 + \tfrac{1}{2\eta}\left\|\mathbf{S}_{n,t}^{\rm low} - \mathbf{S}_{n,t}^{\rm low}(\tau)\right\|^2 \Big). \quad (18)
\end{aligned}$$

Finally, **dual correction** follows the steps in (16), except that the auxiliary variables in the LHS are replaced by $\{\alpha_{n,t}(\tau+1), \gamma_{n,t}(\tau+1), \nu_{n,t}(\tau+1)\}$, and the primal variables in the RHS are replaced by the updated version from (17)-(18).

For the PCPM updates in (16)-(18), each bus only needs to communicate with its *one-hop neighbors*, and the exact convergence of the primal-dual sequences can be rigorously established under the proper choice of stepsizes [17].

Remark 1 (Spatio-temporal decoupling)**.** The current primal steps in (17) and (18) need to solve a *multi-period* convex

[2]Other decentralized solvers such as ADMM [16] can be also applied here.

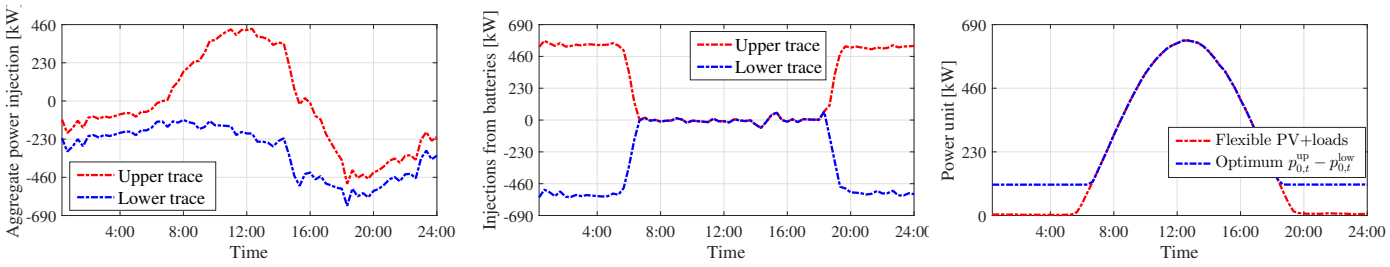

(a) aggregate power injections (b) injections from batteries (c) aggregate flexibility

Fig. 2. Optimal trajectories in the default setting.

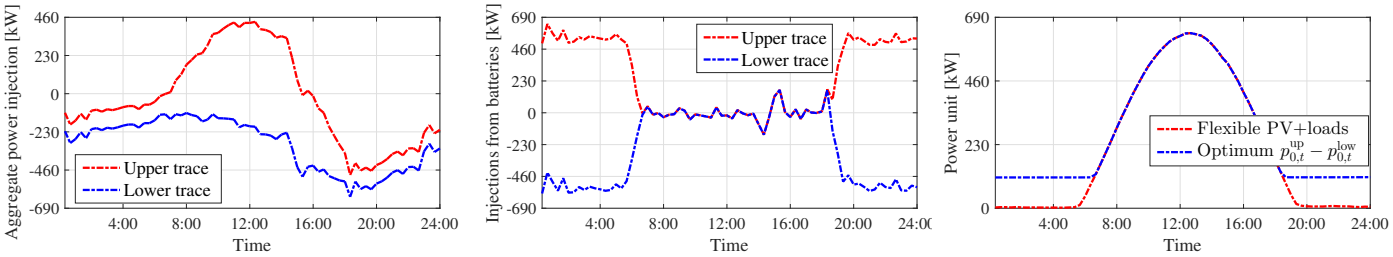

(a) aggregate power injections (b) injections from batteries (c) aggregate flexibility

Fig. 3. Optimal trajectories in the setting with $v_n \in [0.99, 1.01]$ pu.

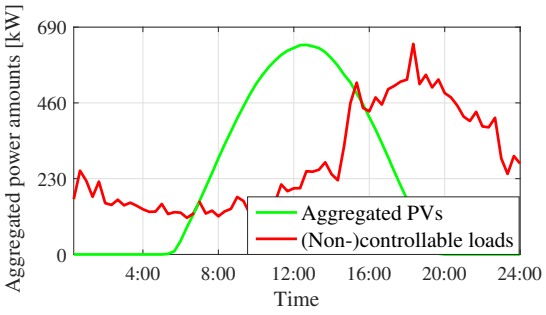

Fig. 4. Real data traces of PV and loads used in simulations.

program at each bus. To further reduce the computation burden, we can introduce additional dual variables associated with the time-coupling battery dynamics in (6a), and the corresponding PCPM updates can be similarly derived. In such a case, the primal step boils down to multiple spatio-temporally decoupled subproblems, where the performance gain comes from the ease of distributed and parallel implementation.

V. Numerical Tests

In this section, we numerically solve the flexibility aggregation problem in (9) using the IEEE 37-bus test system. Specifically, buses 4, 7, 10, 13, 17, 20, 22, 23, 26, 28, 29, 30, 31, 32, 33, 34, 35, and 36 are connected with PV systems, and their generation profile is simulated based on the real solar irradiance data in [18]; and buses 3, 8, 11, 14, 16, 19, 24, and 25 are equipped with batteries, for which the maximum state of charge is 400 kWh, and the (dis)charging rate is 300 kVA. The ratings of PV inverters are 300 kVA for bus 10, 350 kVA for buses 33, 34, and 200 kVA for the remaining inverters. The loads in the original dataset are replaced with real data measured from feeders in Anatolia, CA during the week of August 2012 [18], and the loads at buses 2, 5, 6, 9, 18, 21, and 27 are assumed to be controllable with $\underline{p}^c_{n,t} = 0.9\bar{p}^c_{n,t}$ in (4); see the aggregate real data traces reported in Fig. 4. The voltage limits $\{\bar{v}_n\}$ and $\{\underline{v}_n\}$ are set to 1.05 pu and 0.95 pu, respectively. Line impedances, shunt admittances, and other details on parameters can be found in [6]. We evaluate the allocation performance in terms of the aggregate flexibility at the substation (cf. (8)) over the given horizon of $T = 72$ slots with each slot denoting 20 mins.

For these parameter settings, we first plot the optimal aggregate injections, the aggregate injections from batteries, and the aggregate flexibility in Fig. 2. Interesting enough, the optimal upper trajectory $\{p^{\text{up}}_{0,t}\}$ in Fig. 2(a) has a similar shape as the difference between the PV and load traces in Fig. 4, while the lower one $\{p^{\text{low}}_{0,t}\}$ shares a similar shape with the negative load trace. Intuitively, this is because the upper trajectory intends to admit all the PV generation and curtail all flexible loads, while the lower one is likely to shed all PV and satisfy all flexible loads, as highlighted in Lemma 2. Such intriguing properties can be also inferred from Fig. 2(b), where two trajectories have quite opposite (dis)charging behavior when the PV generation is low, e.g., flexibility needs to be provided by batteries. And the water-filling structure discussed in Lemma 1 can be also observed in Fig. 2(c), where the "flexible PV+loads" curve denotes $R_t := \sum_{n\in\mathcal{N}_{\text{pv}}\cup\mathcal{N}_{\text{cl}}}(p^{\text{up}}_{n,t} - p^{\text{low}}_{n,t})$.

Effect of voltage constraints. To demonstrate the effect of voltage constraints on the optimal trajectories, we test the algorithm under a stricter voltage limit, allowing only 1% deviation from the nominal value. Compared to the corresponding trajectories in Fig. 2, the aggregate power injections as well as the aggregate flexibility in the distribution network remain almost unchanged; see e.g., Figs. 3(a) and 3(c). Under such a strict constraint however, the traces of battery injections in Fig. 3(b) are distorted relative to those in Fig. 2(b), since the batteries have to frequently adjust charging and discharging rates to compensate for the load fluctuations.

Effect of PV flexibility. As PV generation is assumed fully

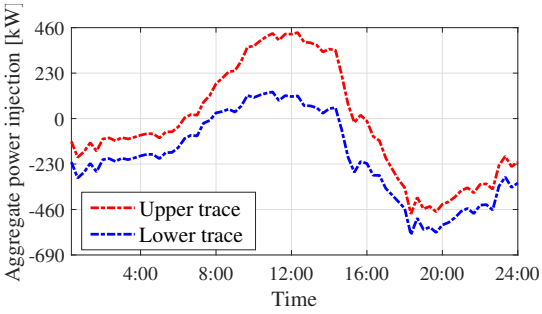

Fig. 5. Optimal trajectories of aggregate injections ($\underline{p}^g_{n,t} = 0.5\bar{p}^g_{n,t}$).

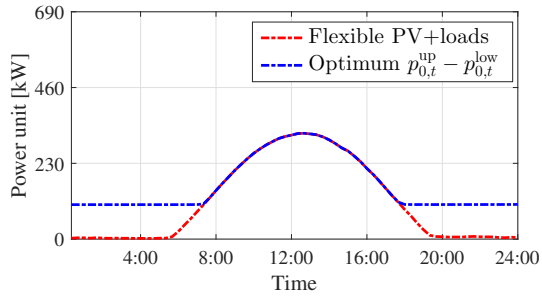

Fig. 6. Optimal trajectories of aggregate flexibility ($\underline{p}^g_{n,t} = 0.5\bar{p}^g_{n,t}$).

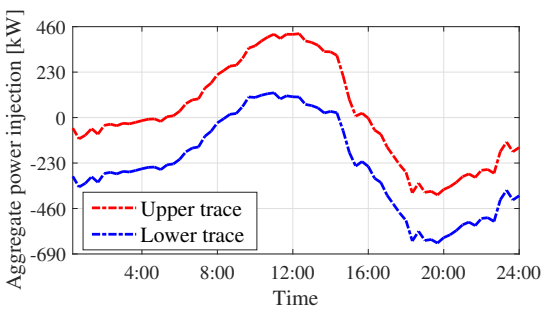

Fig. 7. Optimal trajectories of aggregate injections ($\bar{b}_{n,t} = 1200$ kWh).

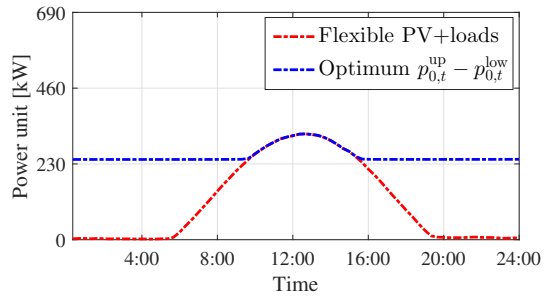

Fig. 8. Optimal trajectories of aggregate flexibility ($\bar{b}_{n,t} = 1200$ kWh).

controllable in the above tests, we have $\underline{p}^g_{n,t} = 0$ in (5). To demonstrate the effect of variable PV flexibility, the optimal trajectories under limited PV flexibility are presented in Figs. 5 and 6; i.e., $\underline{p}^g_{n,t} = 0.5\bar{p}^g_{n,t}$. Relative to those in Figs. 2(a) and 2(c), the aggregate flexibility is lower during the peak sun-hours (cf. Fig. 6). This is because the lower trace also partially admits PV generation, which leads to a larger power injection thus a smaller gap relative to the upper trace (cf. Fig. 5).

Effect of battery size. Figs. 7 and 8 depict the optimal trajectories under larger battery sizes, namely, $\bar{b}_{n,t} = 1200$ kWh with $\underline{p}^g_{n,t} = 0.5\bar{p}^g_{n,t}$. An interesting observation here is that the gap between the upper and lower trajectories in Fig. 7 becomes much more flat, compared to that in Fig. 5. A similar conclusion can be also drawn from Fig. 8, since the flexibility uniformly increases during the off-peak sun-hours. Together with the arguments on flexibility limits in Prop. 1, we deduce that the battery capacity indeed plays an important role in maximizing aggregate flexibility of distribution networks.

VI. Conclusions

In this paper, we studied the optimal flexibility aggregation in distribution networks, including both network-wide constraints, and local operational constraints. By formulating the pertinent optimization problem as a convex program, we revealed several interesting properties of the underlying optimal aggregation solution. Building upon the predictor-corrector proximal multiplier method, we developed a decentralized solver for efficiently finding the optimal aggregation trajectory. Performance of the proposed algorithm was evaluated using the IEEE 37-bus benchmark and the real solar and load measurements.

References

[1] T. Chen, N. Li, and G. B. Giannakis, "Aggregating flexibility of heterogeneous energy resources in distribution networks," Tech. Rep., 2017. [Online]. Available: https://www.dropbox.com/s/54swltoapvy477j/acc2018vonline.pdf?dl=0

[2] G. B. Giannakis, V. Kekatos, N. Gatsis, S.-J. Kim, H. Zhu, and B. F. Wollenberg, "Monitoring and optimization for power grids: A signal processing perspective," *IEEE Signal Processing Mag.*, vol. 30, no. 5, pp. 107–128, 2013.

[3] E. Polymeneas and S. Meliopoulos, "Aggregate modeling of distribution systems for multi-period OPF," in *Proc. Power Syst. Comp. Conf.*, Genoa, Italy, Jun. 2016, pp. 1–8.

[4] V. Kekatos, L. Zhang, G. B. Giannakis, and R. Baldick, "Voltage regulation algorithms for multiphase power distribution grids," *IEEE Trans. Power Syst.*, vol. 31, no. 5, pp. 3913–3923, 2016.

[5] N. Li, G. Qu, and M. Dahleh, "Real-time decentralized voltage control in distribution networks," in *Proc. Allerton Conf.*, Allerton, IL, 2014.

[6] E. Dall'Anese and A. Simonetto, "Optimal power flow pursuit," *IEEE Trans. Smart Grid*, 2017, to appear.

[7] W. Shi, N. Li, X. Xie, C.-C. Chu, and R. Gadh, "Optimal residential demand response in distribution networks," *IEEE J. Select. Areas Commun.*, vol. 32, no. 7, pp. 1441–1450, Jul. 2014.

[8] A. Bernstein, J.-Y. Le Boudec, M. Paolone, L. Reyes-Chamorro, and W. Saab, "Aggregation of power capabilities of heterogeneous resources for real-time control of power grids," in *Proc. Power Syst. Comp. Conf.*, Genoa, Italy, Jun. 2016, pp. 1–7.

[9] M. A. Bucher, S. Chatzivasileiadis, and G. Andersson, "Managing flexibility in multi-area power systems," *IEEE Trans. Power Syst.*, vol. 31, no. 2, pp. 1218–1226, Mar. 2016.

[10] H. Hao, B. M. Sanandaji, K. Poolla, and T. L. Vincent, "Aggregate flexibility of thermostatically controlled loads," *IEEE Trans. Power Syst.*, vol. 30, no. 1, pp. 189–198, Jan. 2015.

[11] L. Zhao and W. Zhang, "A geometric approach to virtual battery modeling of thermostatically controlled loads," in *Proc. American Control Conf.*, Boston, MA, Jul. 2016, pp. 1452–1457.

[12] S. H. Low, "Convex relaxation of optimal power flow, part I: Formulations and equivalence," *IEEE Trans. Control Netw. Syst.*, vol. 1, no. 1, pp. 15–27, May 2014.

[13] W. Shi, N. Li, C.-C. Chu, and R. Gadh, "Real-time energy management in microgrids," *IEEE Trans. Smart Grid*, vol. 8, pp. 228–238, Jan. 2017.

[14] B. Li, T. Chen, X. Wang, and G. B. Giannakis, "Real-time energy management in microgrids with reduced battery capacity requirements," *IEEE Trans. Smart Grid*, 2018, to appear.

[15] L. Gan, U. Topcu, and S. H. Low, "Optimal decentralized protocol for electric vehicle charging," *IEEE Trans. on Power Syst.*, vol. 28, no. 2, pp. 940–951, May 2013.

[16] D. P. Bertsekas and J. N. Tsitsiklis, *Parallel and distributed computation: numerical methods*. Belmont, MA: Athena Scientific, 1997.

[17] G. Chen and M. Teboulle, "A proximal-based decomposition method for convex minimization problems," *Mathematical Programming*, vol. 64, no. 1-3, pp. 81–101, Mar. 1994.

[18] J. Bank and J. Hambrick, "Development of a high resolution, real time, distribution-level metering system and associated visualization, modeling, and data analysis functions," NREL, Tech. Rep., 2013.